UNIVERSITY TRANSPORTATION CENTER FOR RAILWAY SAFETY

The University of Texas Rio Grande Valley

# IMPACT OF HYSTERESIS HEATING OF RAILROAD BEARING THERMOPLASTIC ELASTOMER SUSPENSION PAD ON RAILROAD BEARING THERMAL MANAGEMENT

*The University of Texas Rio Grande Valley (UTRGV)*
*Department of Mechanical Engineering*
*Oscar O. Rodriguez, Graduate Research Assistant*
*Arturo A. Fuentes, Ph.D., Faculty Advisor*
*Constantine M. Tarawneh, Ph.D., UTCRS Director*



# Overview

- Background & Introduction
- Heat Generation Due to Hysteresis Heating
- Experimental Setup
- Heat Transfer Finite Element Modeling
  - Boundary Conditions
- Finite Element Analysis
  - Laboratory Results Validation FEA
  - Suspension Pad Modeling FEA
- Conclusions

# Background & Introduction

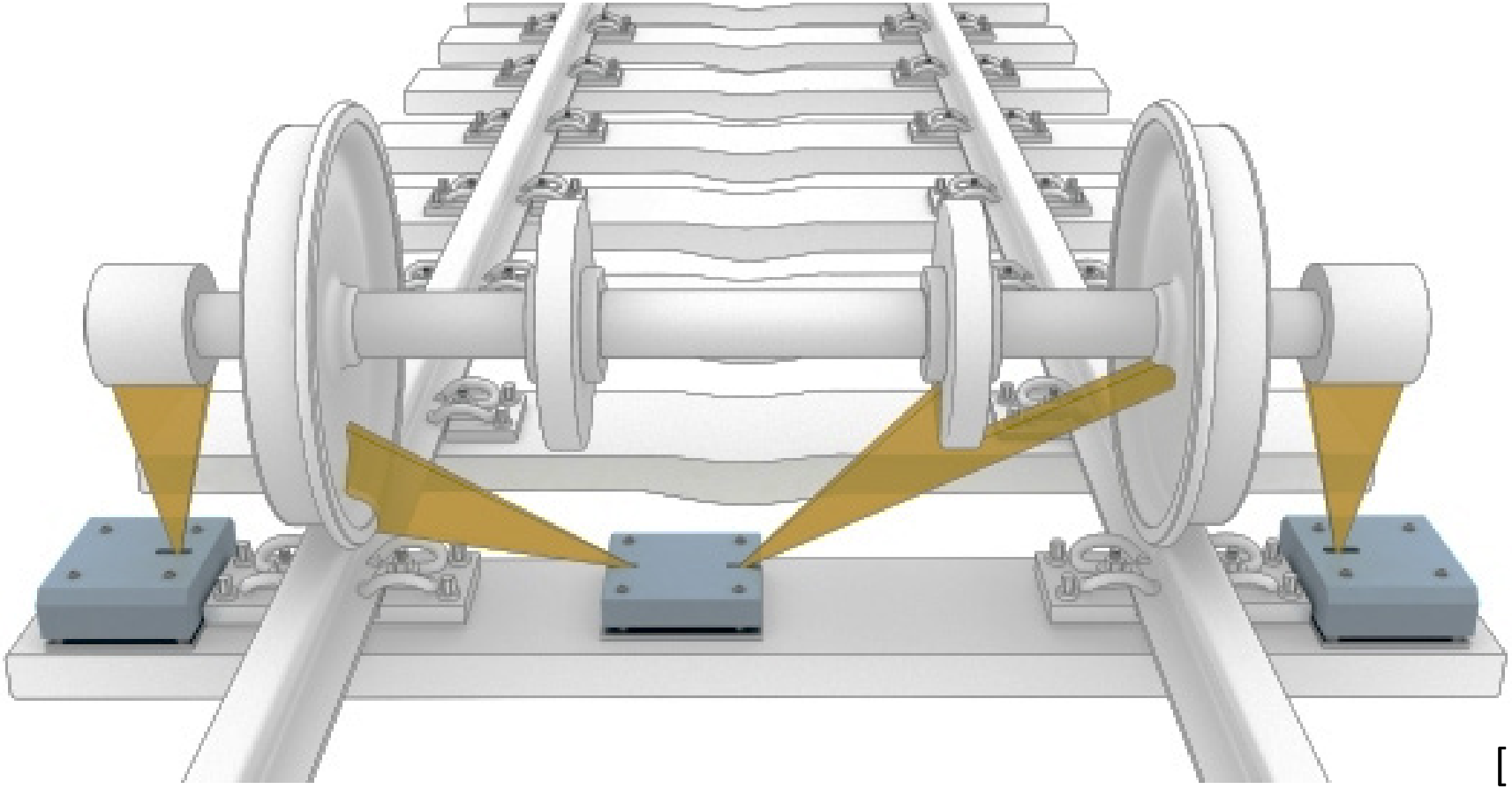

[1]

# Background & Introduction

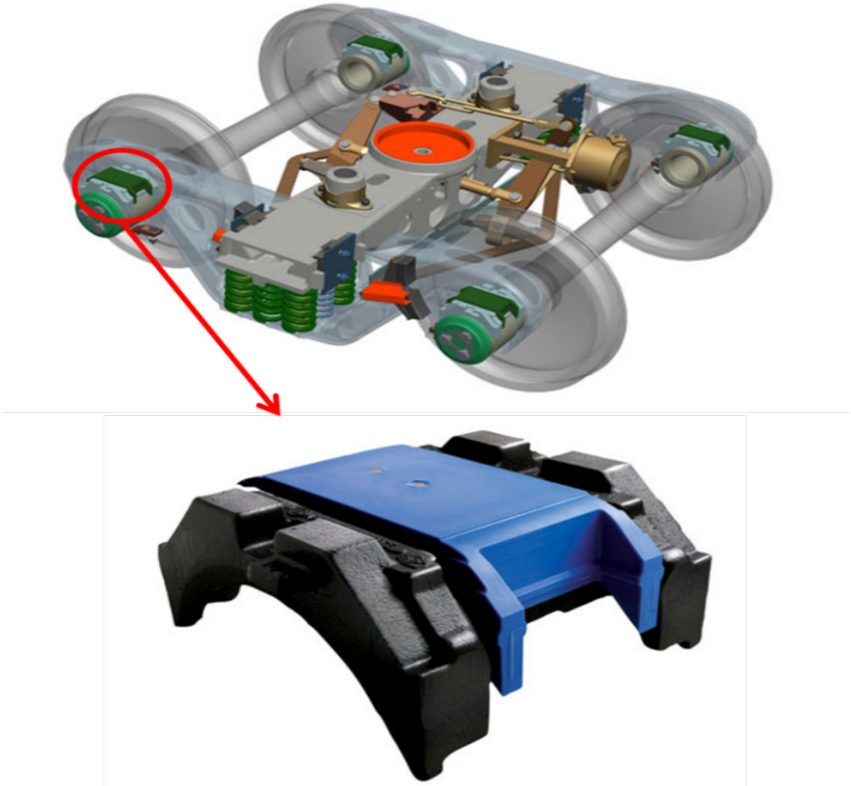

Figure 1. Railroad bearing AdapterPlus™ with elastomer suspension pad [4], [5]

## Thermoplastic Elastomer Suspension Pad

- Prevents metal-to-metal contact between the bearing adapter and the side-frame of the truck.
- Viscoelastic materials are known to develop hysteresis heating under cyclic loading.
- The hysteresis heating is caused by the internal heat generation.

# Heat Generation Due to Hysteresis Heating

- The total heat generation of the material was numerically estimated using dynamic mechanical analysis (DMA) data that were obtained from specimens of the suspension pad material.
- Since the heat generation is a function of the loss modulus, strain percent, and frequency, the following equation can be used with DMA results to calculate specific power ($W/m^3$) dissipated at individual frequencies and temperatures.

$$P = \frac{\omega}{2}\varepsilon_A^2 E''$$

- A loading frequency sweep was done on each specimen ranging from 0.1 to 50 Hz; however, heat generation values were calculated only for frequencies of 10, 20, 30, and 50 Hz.
- The heat generation is also dependent on temperature, and at each frequency, values for the internally generated heat are calculated for temperatures ranging from 30 to 160ºC in increments of 10ºC.

# Heat Generation Due to Hysteresis Heating

| Temperature [°C] | 50 Hz Heat Generation [W/m$^3$] | 30 Hz Heat Generation [W/m$^3$] | 20 Hz Heat Generation [W/m$^3$] | 10 Hz Heat Generation [W/m$^3$] |
|---|---|---|---|---|
| 30 | 14459 | 8053 | 4793 | 2070 |
| 40 | 10441 | 5842 | 3394 | 1428 |
| 50 | 7397 | 4165 | 2369 | 970 |
| 60 | 5065 | 2910 | 1615 | 641 |
| 70 | 3463 | 2068 | 1123 | 428 |
| 80 | 2493 | 1537 | 821 | 300 |
| 90 | 1836 | 1219 | 641 | 228 |
| 100 | 1457 | 1004 | 529 | 184 |
| 110 | 1191 | 859 | 455 | 155 |
| 120 | 1045 | 808 | 405 | 137 |
| 130 | 931 | 737 | 375 | 121 |
| 140 | 873 | 716 | 350 | 111 |
| 150 | 888 | 748 | 338 | 106 |
| 160 | 860 | 781 | 313 | 100 |

Table 1. Calculated heat generation values

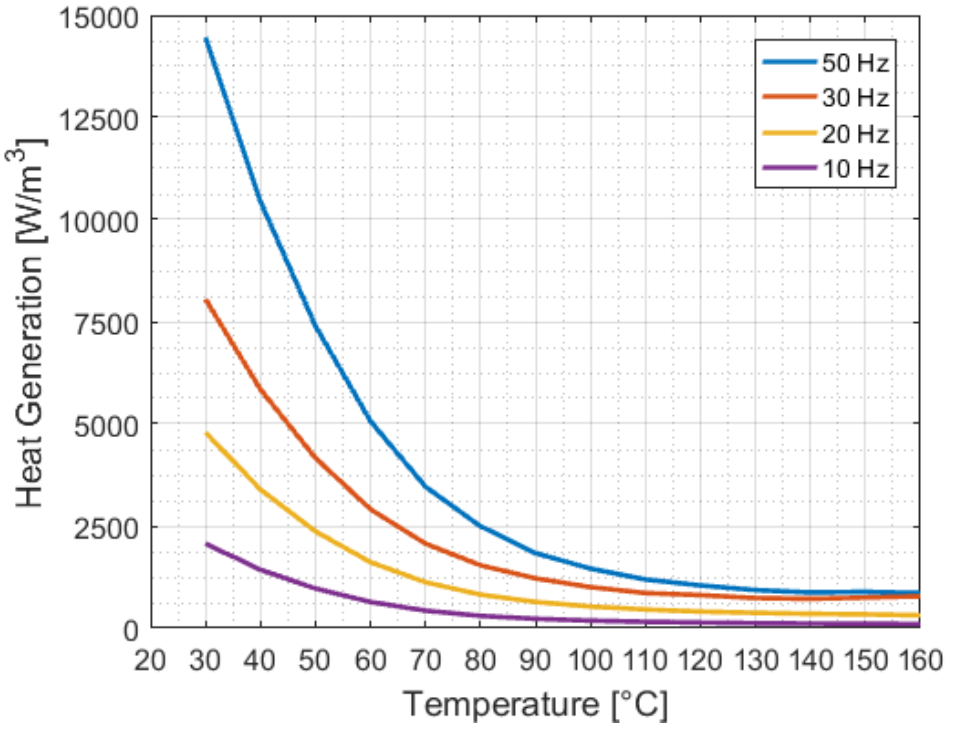


Figure 2. Heat generation curves at different loading frequencies

# Experimental Setup

**Four Bearing Dynamic Test Rig (4BT)**

Figure 3. Four Bearing Tester (4BT)

**Single Bearing Dynamic Test Rig (SBT)**

Figure 4. Single Bearing Tester (SBT)

# Experimental Setup

## Four Bearing & Single Bearing Dynamic Test Rigs

- The test rigs are specifically designed to closely mimic railroad service operation conditions which a railroad bearing experiences.
- A fully-loaded railcar (100% load) corresponds to an applied load of 153 kN (34.4 kips) per bearing for Class F and Class K bearings, whereas, an empty railcar (17% load) corresponds to an applied load of 26 kN (5.85 kips).
- Capable of applying vertical loads ranging from 0 to 175% of full-load utilizing a hydraulic cylinder.
- Utilizes a variable-speed motor powered by a variable-frequency drive (VFD), which simulates train speeds ranging from 5-137 km/h (or 8-85 mph).
- Two industrial strength fans are used to produce an average air stream of 18 km/h (11.2 mph).

# Heat Transfer Finite Element Modeling

- A computer aided design (CAD) model was created and constructed in SolidWorks™, which was then imported into ALGOR 20.3™ to create a finite element model for the heat transfer analysis.

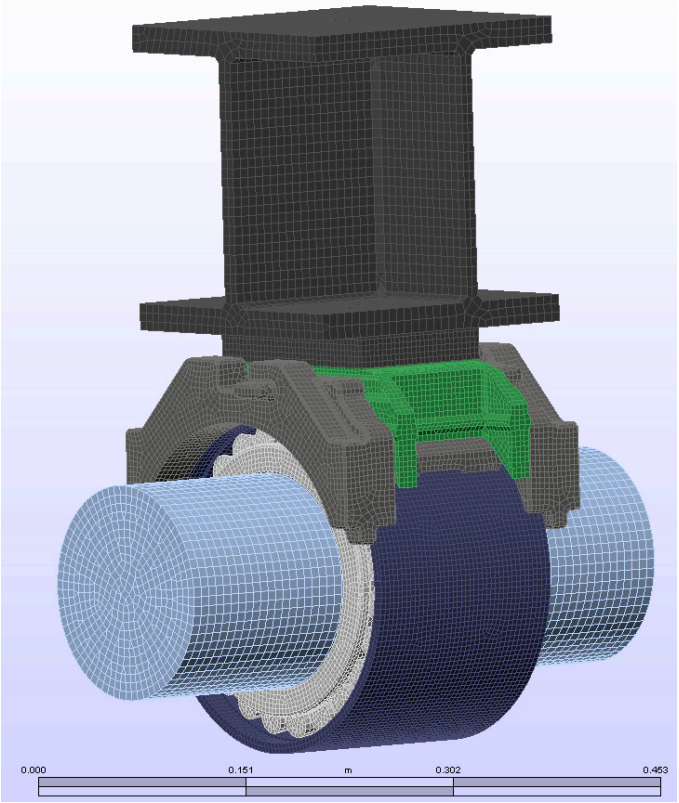


Figure 5. Complete laboratory bearing assembly FEA model

# Heat Transfer Finite Element Modeling

- Four major boundary conditions were applied: conduction, convection, heat flux, and heat generation.
- Since the mass of the roller is very small compared to the mass of the cup and cone, it is safe to assume that it will heat at a much faster rate than the other two components, thus, becoming the heat source.
- Since this is a static model, the actual rotation of the cone assemblies inside the bearing was not directly simulated, but was taken into account by applying an average heat flux through all 46 rollers in the bearing.

# Heat Transfer Finite Element Modeling

- Thermal contact resistance between the adapter and bearing cup may significantly affect the amount of heat transferred to the bearing adapter.
- A thermal contact resistance of 0.0055 $m^2 \cdot K \cdot W^{-1}$ was applied in between the bearing cup and adapter (obtained experimentally).
- In order to model both heat sources simultaneously (i.e. the heat flux of the rollers and the heat generation of the suspension pad), a thermal contact resistance of 0.01 $m^2 \cdot K \cdot W^{-1}$ was applied between the suspension pad and the metal adapter, and between the suspension pad and the I-beam spacer plate.


# Heat Transfer Finite Element Modeling

## Cup

- An overall heat transfer coefficient $H_o = 8.32\ \mathrm{W \cdot K^{-1}}$ is provided for the bearing cup, however, the software appropriate units require the aforementioned convection value to be divided by the bearing cup surface area ($A_{cup} = 0.1262\ \mathrm{m^2}$), leading to a cup convection coefficient $h_o = 65.9\ \mathrm{W \cdot m^{-2} \cdot K^{-1}}$.

## Axle

- The convection coefficient was obtained by using the Nusselt number correlation for a cylinder in cross-flow. A resulting value of $h_{axle} = 25\ \mathrm{W \cdot m^{-2} \cdot K^{-1}}$ is obtained.

## Other Components

- For the adapter, adapter pad, I-beam, and spacer plate, the convection coefficient values were obtained by using the Nusselt number correlation for a flat plate in parallel flow.

# Heat Transfer Finite Element Modeling

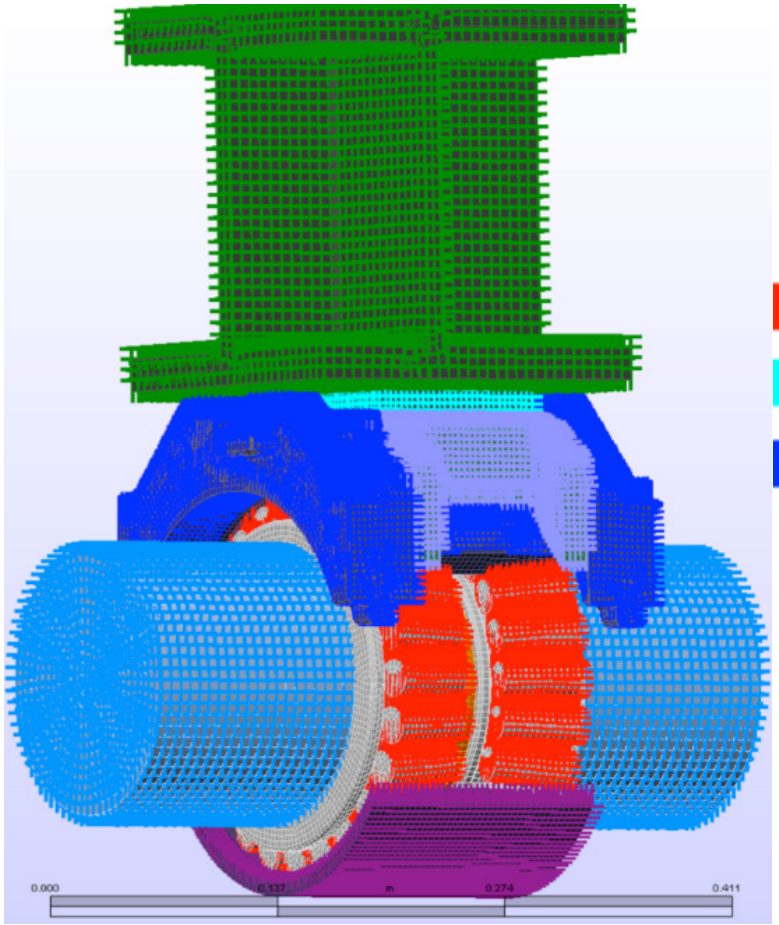


Roller heat flux

Spacer plate convection ($18.3\ W \cdot m^{-2} \cdot K^{-1}$)

AdapterPlus™ convection ($17.9\ W \cdot m^{-2} \cdot K^{-1}$)

I-beam convection ($19.0\ W \cdot m^{-2} \cdot K^{-1}$)

Adapter pad convection ($17.9\ W \cdot m^{-2} \cdot K^{-1}$)

Axle convection ($25.0\ W \cdot m^{-2} \cdot K^{-1}$)

Bearing cup overall convection ($65.9\ W \cdot m^{-2} \cdot K^{-1}$)

Figure 6. Boundary conditions applied to each FE model component

# Heat Transfer Finite Element Modeling

| Part | $h_{avg}$ [W·m$^{-2}$·K$^{-1}$] |
|---|---|
| I-beam | 19.0 |
| Spacer Plate | 18.3 |
| AdapterPlus™ | 17.9 |
| Adapter Pad | 17.9 |
| Overall Average | 18.1 |

Table 2. Convection coefficient values for each FE model component

| **Operation Condition** | **Ambient Temp. [°C]** | **Load [%]** | **Train Speed [km/h] / [mph]** |
|---|---|---|---|
| ***Normal*** | 25 | 100 | 96.6 / 60 |
| ***Abnormal*** | 45 | 100 | 137 / 85 |

Table 3. Laboratory operation conditions for FEA comparison

# Finite Element Analysis

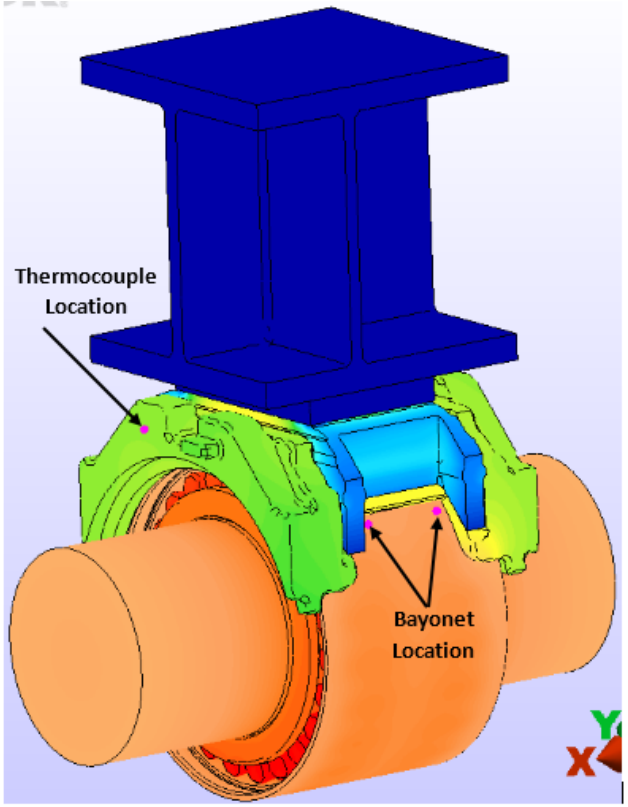


Figure 7. AdapterPlus™ FE model with nodes of interest indicated

- FE model with markers showing the location of the selected nodes
- The same reference temperature locations on the adapter were used for comparison and model validation
- Determined that the results of the complete FE model developed for this study matched the experimental results

# Finite Element Analysis

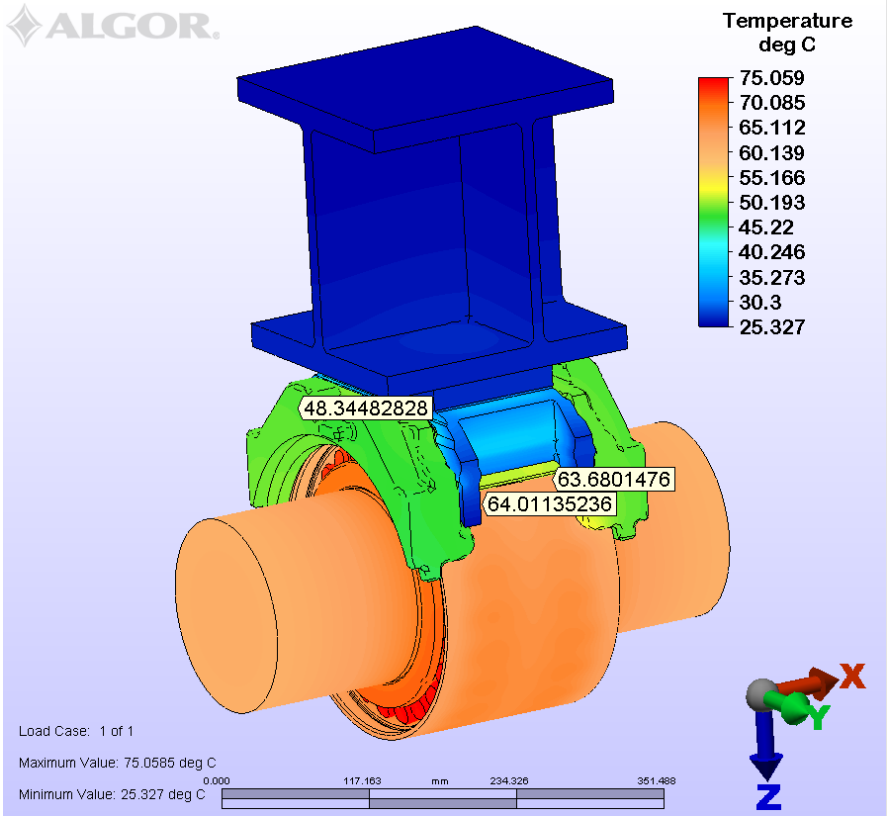


Figure 8. Temperature distribution with normal operation conditions and no heat generation

| *Normal Operation Conditions* | | |
|---|---|---|
| **Source of Results** | **Thermocouple [°C]** | **Bayonet [°C]** |
| Experimental | 44.2 | 65.4 |
| FEA | 48.4 | 64.1 |
| % Difference | 9.5 | 2 |

Table 4. Experimental and FEA results comparison

# Finite Element Analysis

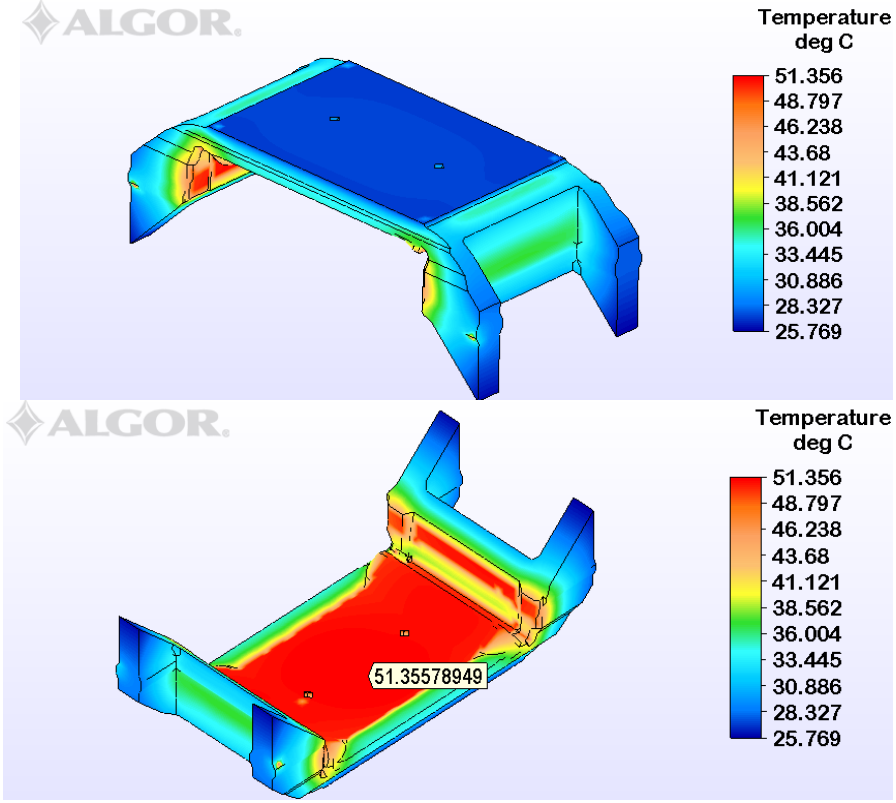


Figure 9. Top and bottom surface temperature distribution and maximum temperature of the suspension pad with normal operation conditions

- The figure demonstrates that most of the heat from the adapter is dissipated by convection along the sides of the adapter, while significantly less heat is dissipated by conduction through the central rectangular area on the bottom surface of the suspension pad.
- It is evident that most of the heat is partially insulated from the I-beam and spacer plate.

# Finite Element Analysis

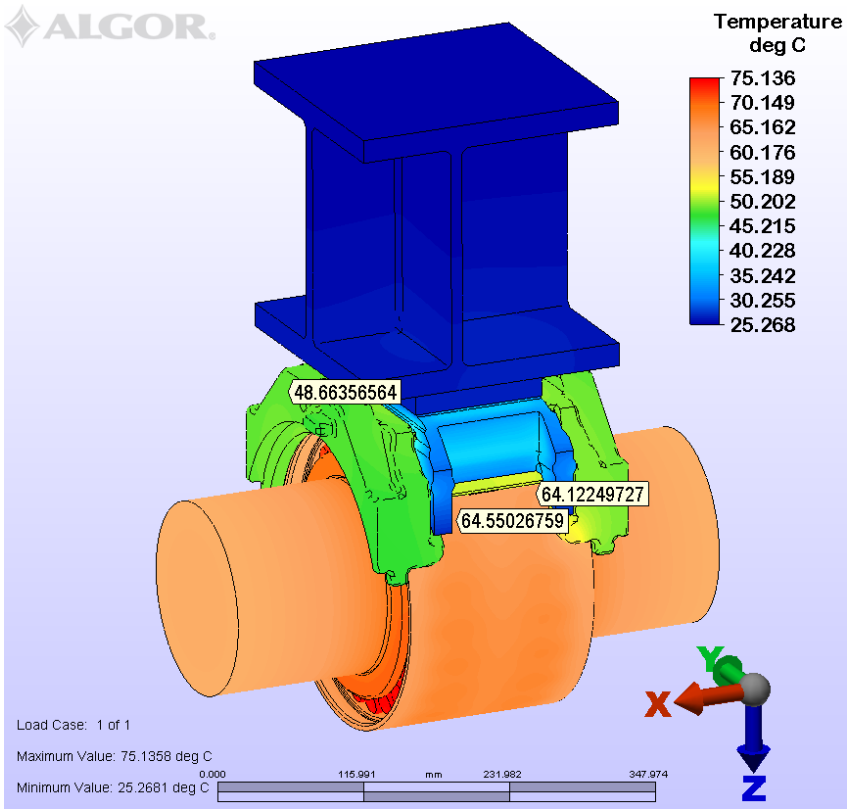


Figure 10. AdapterPlus™ FE model with an applied heat generation due to a frequency loading of 10 Hz and normal operation conditions

- Compared to the simulation results presented for the FEA model with no applied heat generation, the results show almost no change in the temperature distribution of the bearing assembly, adapter, or suspension pad.
- Although the maximum pad temperature is nearly the same for the two simulations (i.e. with and without pad heat generation), the temperature distribution within the pad differs markedly.
- Comparing the two simulations, it can be observed that the maximum temperature at the bottom surface shifts from the center of the pad (Figure 9) to the pad interlocks (Figure 11). Also the temperature of the top surface of the pad is warmer.

# Finite Element Analysis

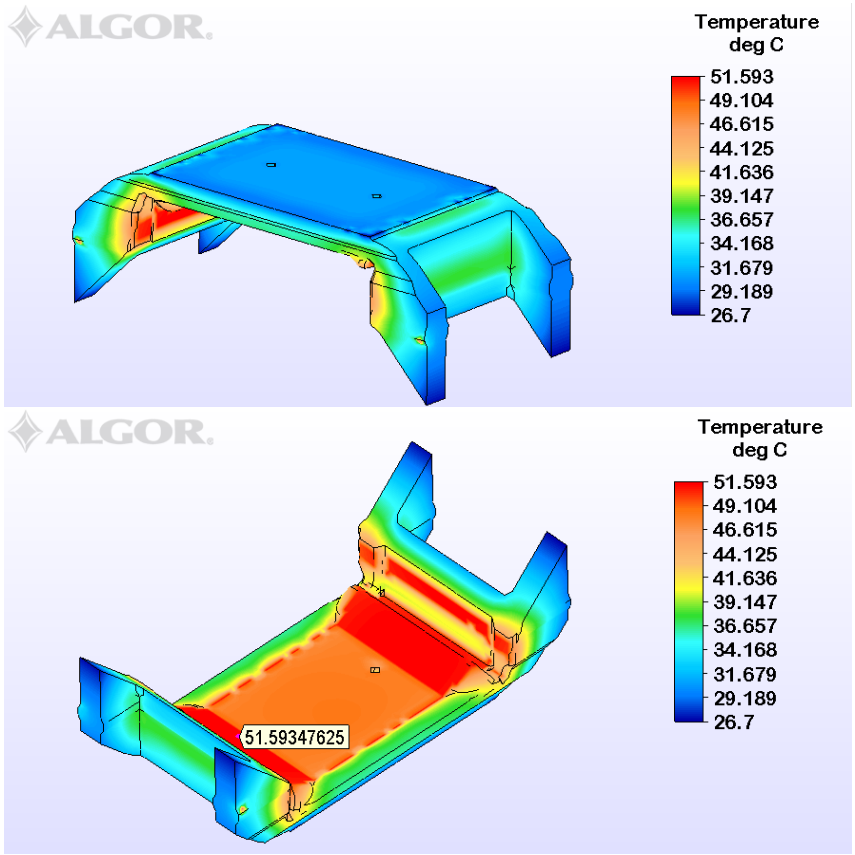


| *Normal Operation Conditions* | | | |
|---|---|---|---|
| **Operation Condition** | **Bayonet [°C]** | **Thermocouple [°C]** | **Pad [°C]** |
| Heat Generation | 64.4 | 48.9 | 51.6 |
| No Heat Generation | 64.1 | 48.4 | 51.4 |
| **ΔT [°C]** | 0.3 | 0.5 | 0.2 |

Table 5. AdapterPlus™ FE model temperature comparison (no pad heat generation versus 10 Hz pad heat generation)

Figure 11. Top and bottom surface temperature distribution and maximum temperature of the suspension pad with normal operation conditions and an applied constant heat generation due to a frequency loading of 10 Hz

# Finite Element Analysis

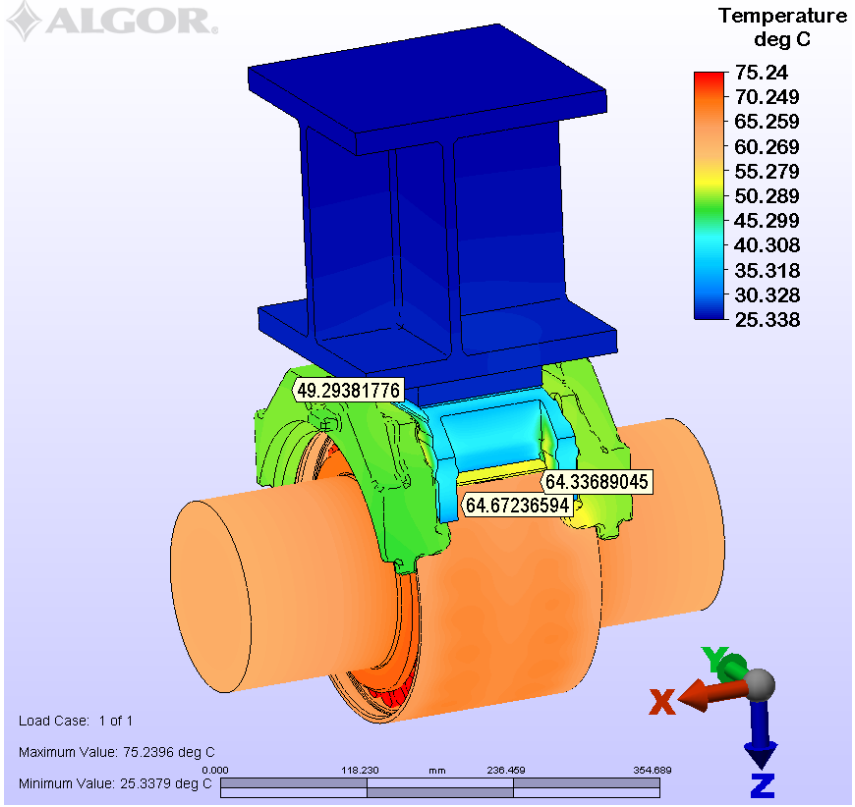


Figure 12. AdapterPlus™ FE model with an applied heat generation due to a frequency loading of 50 Hz and normal operation conditions

- The results of this simulation compared to those in (Figure 8) and (Figure 10) show that the higher applied pad heat generation hardly affects the temperature distribution of the bearing assembly or the adapter.
- Figure 13 shows that the maximum temperature of the pad increases by 4°C, and the region of maximum temperature at the bottom surface of the pad shifts to the pad legs.

# Finite Element Analysis

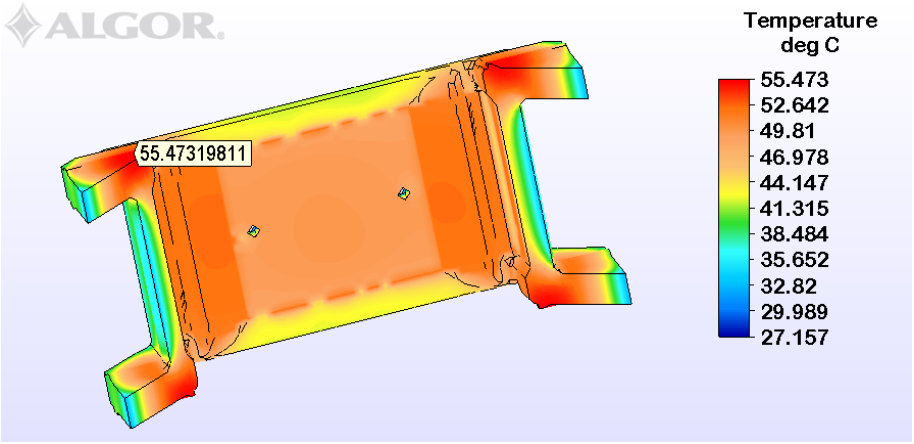


Figure 13. Bottom surface temperature distribution and maximum temperature of the suspension pad with normal operation conditions and an applied constant heat generation due to a frequency loading of 50 Hz

| *Normal Operation Conditions* | | | |
|---|---|---|---|
| **Operation Condition** | **Bayonet [°C]** | **Thermocouple [°C]** | **Pad [°C]** |
| Heat Generation | 64.5 | 49.3 | 55.5 |
| No Heat Generation | 64.1 | 48.4 | 51.4 |
| **ΔT [°C]** | 0.4 | 0.9 | 4.1 |

Table 6. AdapterPlus™ FE model temperature comparison (no pad heat generation versus 50 Hz pad heat generation)

# Conclusions

- The results show that in normal and abnormal operation conditions, the internal heat generation in the thermoplastic elastomer suspension element has limited impact on the thermal behavior of the railroad bearing assembly as long as the pad is able to dissipate heat through the side frame of the truck.
- The AdapterPlus™ FE model also shows that with normal operation conditions, the temperature distribution of the suspension pad remains relatively the same when heat generation is applied. However, the constant heat generation due to a frequency loading of 50 Hz does cause the maximum temperature of the pad to increase by about 4°C.
- Although this minor increase in temperature is not significant to the temperature distribution of the suspension pad nor does it significantly impact the thermal management or temperature distribution of the bearing assembly, the results indicate that if a significant amount of energy is generated by the suspension pad with no thermal runway, it can highly impact the structural integrity of the suspension pad.
- In fact, previous results show that a combination of the ambient temperature, bearing temperature, and frequency of loading can produce elastomer pad temperature increases above ambient of up to 125°C when no thermal runway is present.

# Acknowledgments

This study was made possible by funding provided by The University Transportation Center for Railway Safety (UTCRS), through a USDOT Grant No. DTRT 13-G-UTC59. The authors also gratefully acknowledge the assistance provided by Mr. Joseph Montalvo and Mr. James Aranda.

# References

1. "Hot Box & Hot Wheel Detection System." HOT BOX & HOT WHEEL DETECTION SYSTEM. Web. 28 Mar. 2016. <http://www.mermecgroup.com/inspection-technology/hot-box-detector-/418/1/hot-box-detector-.php>.
2. Tarawneh, C. M., Cole, K. D., Wilson, B. M., & Alnaimat, F. (2008). Experiments and models for the thermal response of railroad tapered-roller bearings. *International Journal of Heat and Mass Transfer*, 51(25-26), 5794-5803. Retrieved March 13, 2016.
3. Tarawneh, C., et al. "Thermal Modeling of a Railroad Tapered-Roller Bearing Using Finite Element Analysis." *Journal of Thermal Science and Engineering Applications*, vol. 4, no. 3, pp. 9-19, 2012.
4. "Truck Assemblies | Amsted Rail." *Truck Assemblies | Amsted Rail*. Web. 28 Mar. 2016. <http://www.amstedrail.com/products-services/truck-assemblies>.
5. "Adapter Plus Steering Pad System | Amsted Rail." *Adapter Plus Steering Pad System | Amsted Rail*. Web. 28 Mar. 2016. <http://www.amstedrail.com/products-services/adapter-plus-steering-pad-system>.
6. Zagouris, A., Fuentes, A. A., Tarawneh, C. M., Kypuros, J. A., & Arguelles, A. (2012). Experimentally Validated Finite Element Analysis of Railroad Bearing Adapter Operating Temperatures. *Volume 7: Fluids and Heat Transfer, Parts A, B, C, and D*.